Article

A Comparative Biochemical and Pathological Evaluation of Brain Samples from Knock-in Murine Models of Gaucher Disease

Makaila Furderer , Bahafta Berhe , Tiffany Chunwei Chen , Stephen Wincovitch , Xuntian Jiang , Nahid Tayebi , Ellen Sidransky [*] , Tae-Un Han [*]

Article

A Comparative Biochemical and Pathological Evaluation of Brain Samples from Knock-in Murine Models of Gaucher Disease

Makaila L. Furderer [1,4], **Bahafta Berhe** [1,4], **Tiffany Chen** [1,4], **Stephen Wincovitch** [2], **Xuntian Jiang** [3], **Nahid Tayebi** [1,4], **Ellen Sidransky** [1,4]* **and Tae Un Han** [1,4]*

[1]Medical Genetics Branch, National Human Genome Research Institute, National Institutes of Health, Bethesda, Maryland, USA

[2]Microscopy Core, National Human Genome Research Institute, National Institutes of Health, Bethesda, Maryland, USA

[3]Washington University Metabolomics Facility, Washington University School of Medicine, St. Louis, Missouri, USA

[4]Aligning Science Across Parkinson's (ASAP) Collaborative Research Network, Chevy Chase, MD 20815

*Correspondence: Dr. Ellen Sidransky and Dr. Tae Un Han, Section on Molecular Neurogenetics, MGB, National Human Genome Research Institute, Building 35A, Room 1E623, 35A Convent Drive, MSC 3708, Bethesda, MD 20892-3708; Emails: sidranse@nih.gov and Taeun.han@nih.gov

Abstract: Gaucher disease (GD) is a lysosomal storage disorder stemming from biallelic mutations in *GBA1*, characterized by glucocerebrosidase dysfunction and glucocerebroside and glucosylsphingosine accumulation. Since phenotypes of murine models of GD often differ from those in patients, careful characterization of *Gba1* mutant mice is necessary to establish their ability to model GD. We performed side-by-side comparative biochemical and pathologic analyses of four murine *Gba1* models with genotypes L444P/L444P (p.L483P/p.L483P), L444P/null, D409H/D409H (p.D448H/p.D448H), and D409H/null, along with matched wildtype mice, all with the same genetic background and cage conditions. All mutant mice exhibited significantly lower glucocerebrosidase activity (p < 0.0001) and higher glucosylsphingosine levels than wildtype, with the lowest glucocerebrosidase and highest glucosylsphingosine levels in mice carrying a null allele. Although glucocerebrosidase activity in L444P and D409H mice was similar, D409H mice showed more lipid accumulation. No Gaucher or storage-like cells were detected in any of the *Gba1* mutant mice. Quantification of neuroinflammation, dopaminergic neuronal loss, alpha-synuclein levels and motor behavior revealed no significant findings, even in aged animals. Thus, while the models may have utility for testing the effect of different therapies on enzymatic activity, they did not recapitulate the pathological phenotype of patients with GD, and better models are needed.

Keywords: Gaucher disease; glucocerebrosidase; neuropathology; glucosylsphingosine; murine models; Parkinson disease

1. Introduction

Gaucher disease (GD), a prevalent lysosomal storage disorder, is caused by biallelic mutations in *GBA1*, the gene encoding the lysosomal enzyme glucocerebrosidase (GCase). GCase is responsible for catalyzing the hydrolysis of the glycolipids glucosylceramide (GlcCer) and glucosylsphingosine (GlcSph). When GCase activity is deficient, these lipid substrates accumulate, resulting in engorged macrophages known as Gaucher cells, a hallmark of the disease. Mutations in *GBA1* are also the most common risk factor for the development of Parkinson disease (PD). Clinical studies noting patients with GD and early onset PD led to the discovery of this intriguing relationship [1, 2]. There is a broad range of clinical presentations in GD, extending from severe and rapidly progressive neurodegeneration in infancy to patients with extensive skeletal or visceral disease to largely asymptomatic cases identified in the elderly [3, 4]. Animal models that accurately reproduce the phenotypes observed in the different types of human GD are essential for understanding this heterogeneity, as well as for developing and testing the efficacy of novel therapeutics [5].

Mouse models of GD have been challenging to generate as they often fail to produce the same phenotype observed in human disease [6, 7]. A total knockout of glucocerebrosidase leads to a neonatal lethal phenotype with impaired skin ultrastructure, analogous to the most severe neonates with type 2 GD [8]. Fortunately, other strategies have been used to establish models that more closely resemble most patients with acute neuronopathic GD (nGD) or chronic nGD. The K14-lnl/lnl line was developed to circumvent the lethal skin phenotype observed in other KO models [9]. Neuropathological evaluation confirmed prominent abnormalities, making this a useful model for testing therapeutics. Pewzner-Jung et al. (2021) developed a mouse model by utilizing doxycycline to regulate the expression of a *Gba* transgene to generate *Gba*$^{-/-}$; *Gbatg* mice that phenotypically modeled type 3 GD, displaying GlcCer accumulation, neuronal loss, and gliosis [10]. Several other nGD models were also generated, but the mice either died perinatally or were viable but lacked symptoms analogous to those seen in patients with GD [11]. In addition to the failure of many of the models to recapitulate human GD phenotypes, some available models such as D409V (D448V) mice do not carry mutations commonly found in patients [11].

In humans, homozygosity for the L444P (p.L483P) mutation is usually associated with type 3 nGD [3]. Neuronal loss and degeneration are the most common neuropathological features of human nGD [12, 13]. Early attempts to create a L444P murine model by introducing a duplicated mutant allele resulted in mice that died after 1-2 days [14]; subsequently it was shown that mice homozygous for L444P with the WT version of the *Ugcg* gene actually had a normal lifespan [15]. Several studies have established that while GCase activity in homozygous mice is ~20% of WT [14-16], the mice do not accumulate GlcCer. Associated symptoms include inflammation, anemia, leukopenia, skin abnormalities and reduced serum cholesterol levels [15]. Crossing these L444P mice with a *Gba* KO model resulted in *Gba* L444P/null mice which had greatly reduced GCase enzyme activity, elevated GlcSph levels and GlcCer accumulation by 6 months [17]. A second L444P/L444P mouse was generated by targeted homologous recombination. While these mice have a normal lifespan and breed well, observed histopathology included Gaucher cells in viscera and mild astrogliosis [18]. Data on behavioral testing, especially regarding motor function has not been published on any L444P homozygous mice; only Fishbein et al. (2014) evaluated motor function in the Liu model, but in mice also harboring the A53T mutation in *SNCA*.

Another relatively common GD mutation is D409H (p.D448H). GCase with mutation D409H is catalytically defective, susceptible to proteolytic digestion, and unstable [19]. In humans, homozygosity for D409H induces a unique phenotype consisting of oculomotor abnormalities, hydrocephalus, and valvular/aortic calcifications [20, 21]. Unfortunately, mice with genotypes D409H/D409H and D409H/null failed to display the phenotype detected in human GD patients. Mice homozygous for D409H lack central nervous system (CNS) pathology and have a normal lifespan [13, 22]. Low levels of GlcCer accumulation in tissues other than the brain were observed [19, 22]. Subsequently, Xu et al. (2003) crossed homozygous D409H/D409H animals with null/WT animals to produce D409H/null mice. Gaucher cells in the spleen lungs and liver appeared 3-4 months earlier in the D409H/null animals, but no GlcCer accumulation was observed in the brain in either model, and they did not display CNS abnormalities phenotypically or histologically [19].

An ongoing need in this field is an appropriate mouse model for assessing the impact of drug interventions targeting the brain. Since it is difficult to compare mutant mice that were generated with diverse mutations and strategies, and in different facilities, we decided to evaluate a panel of mice in parallel using the same breeding and caging conditions, animal care, and pathology assessments, focusing on a direct comparison of the L444P and D409H homozygous models in our colony. In addition, through cross breeding we generated compound heterozygotes with either a L444P or D409H allele and a null allele. We studied the phenotypes of mice with genotypes wildtype (WT), *Gba*$^{L444P/L444P}$(LP/LP), *Gba* $^{D409H/D409H}$ (DH/DH), *Gba*$^{L444P/null}$ (LP/null)- and *Gba*$^{D409H/null}$ (DH/null) side-by-side, evaluating markers of astrogliosis, microgliosis, the density of dopaminergic neurons and α-synuclein levels and aggregation. Some lines also underwent behavioral testing. Based on data from previous studies, we hypothesized that the haploinsufficient/point mutant mice might better

model chronic neuronopathic GD or *Gba*-associated PD and have enhanced utility for therapeutic development.

2. Results

2.1. Evaluation of GCase pathology in Gba mutant mice

GCase activity was significantly reduced in LP/LP and DH/DH mice (Figure 1a,b) in both the brain and the liver. The combination of a null allele and a point mutation resulted in lower GCase activity than that seen in homozygous L444P and D409H point mutations in brain lysates, and this trend was also observed in liver lysate, although neither reached statistical significance. The fluorescence and enzyme activity assay data are available in Zenodo at DOI: 10.5281/zenodo.10431006. Lipid analysis showed that none of the models accumulated GlcCer (Figure 1d and 1f). Each of the *Gba* mutant models had higher levels of GlcSph than WT in both brain and liver (Figure 1c and 1e). The LP/LP and DH/DH mice showed a 6-fold and 17-fold increase of GlcSph in brain respectively, while the LP/null and DH/null mice showed 16-fold and 35-fold increase of GlcSph in brain respectively. This data indicates that in these models the D409H mutation has a greater impact on GlcSph accumulation than the L444P mutation, and that the combination of a null allele and point mutations increased the lipid accumulation compared to mice with homozygous point mutations. This trend was also observed in liver, where the impact of D409H on GlcSph accumulation was greater than L444P, and hepatic GlcSph levels were higher than in brain (Figure 1e). The lipid analysis data are available in Zenodo at DOI:10.5281/zenodo.10431187.

Immunoblotting showed double bands for the GCase protein, where the upper band was arround 60 kDa, which corresponds the molecular weight of glycosylated GCase, and the lower 50 kDa band likely represents deglycosylated GCase. The combined quantification of both bands showed no signficant difference inf total GCase levels between the different *Gba* genotypess (Figure 1h). However, quantification of the glycosylated GCase band showed that the GCase levels in LP/null and LP/LP were significantly lowered than wildtype GCase (Figure 1i), while in DH/DH and DH/null mice levels were not different from wildtype (Figure 1i). This data indicates that the GCase protein levels alone are not driving the GlcSph levels. Also, the western blots suggest that the L444P mutant form of GCase is more deglycosylated than wildype GCase. All the immunoblot quatification data are available in Zenodo at DOI: 10.5281/zenodo.10431048.
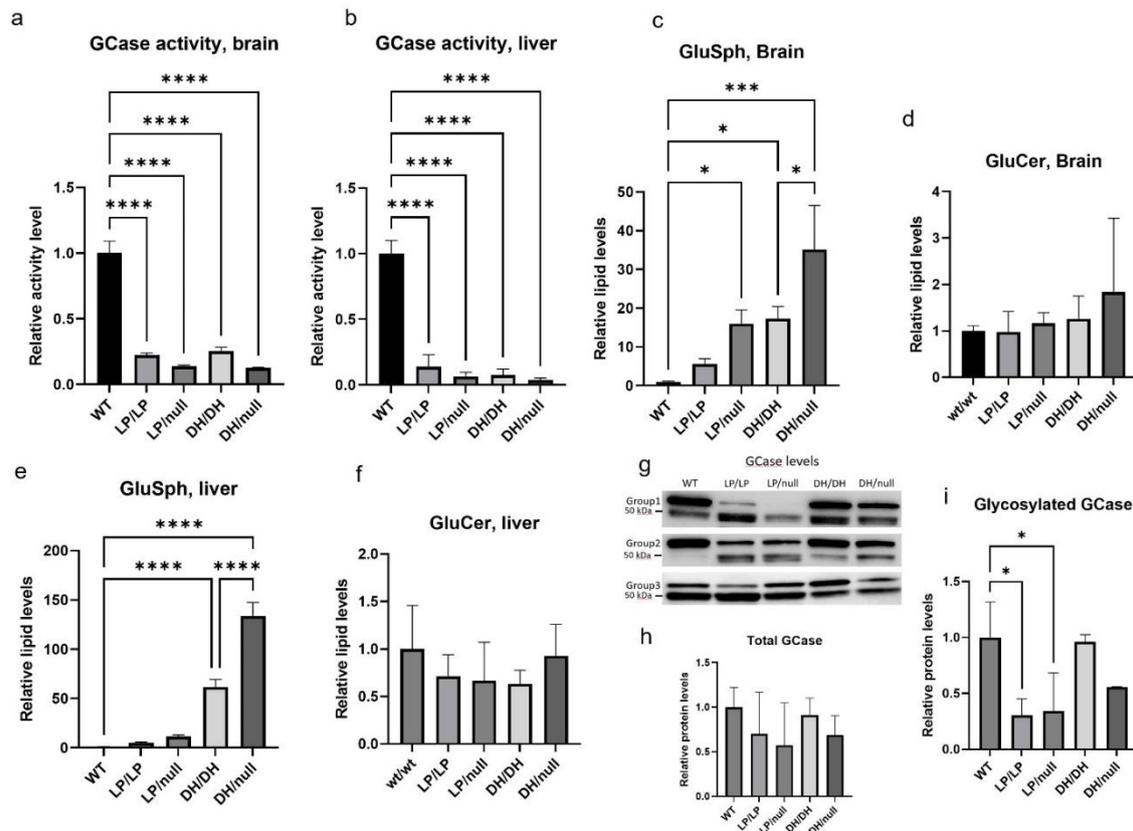
Figure 1. Evaluation of glucocerebrosidase activity, protein levels, and glycolipid levels in *Gba* mutant mice. All assays were conducted in tissue lysates from either wildtype (WT), *Gba*^*L444P/L444P*^ (LP/LP), *Gba*^*L444P/null*^(LP/null), *Gba*^*D409H/D409H*^(DH/DH), and *Gba*^*D409H/null*^ (DH/null) animals at age six month. (a) Relative GCase activity in brain lysates. (b) Relative GCase activity in liver lysates (c) Relative levels of glucosylsphingosine in brain lysates. (d) Relative levels of glucosylceramide in brain lysates. (e) Relative levels of glucosylsphingosine in liver lysates. (f) Relative levels of glucosylceramide in liver lysates. (g) Immunoblotting for evaluation of GCase levels in RIPA using brain lysates. (h) Quantification of immunoblot band intensity for bands combined (i) Quantification of immunoblot band intensity for the high molecular weight band. Intensity of each immunoblot band was normalized by total protein of the same lane measured by Ponceau-S staining. All the assays were repeated in three different animals for each genotype group and then averaged. Error bars indicate the standard deviation. One way ANOVA with Sidak's multiple comparison test was the statistical method used. *$p < 0.05$; **$p < 0.01$; ***$p < 0.001$; ****$p < 0.0001$.

*2.2. Evaluation of Visceral Pathology of Gba mutant mice*

To evaluate visceral pathology in the four *Gba* mutant mice, liver and spleen were collected from 6-month-old mice and H&E staining was performed on transverse section of each tissue. No Gaucher cells were observed in the liver or spleen in mice with any of the four *Gba* genotypes. (data not shown). To determine whether additional maturation of the mice was needed for the development of pathological cells, we repeated the evaluations using 14-month-old mice. However, again we did not detect Gaucher cells in the liver and spleen of the older mutant mice (Figure 2).
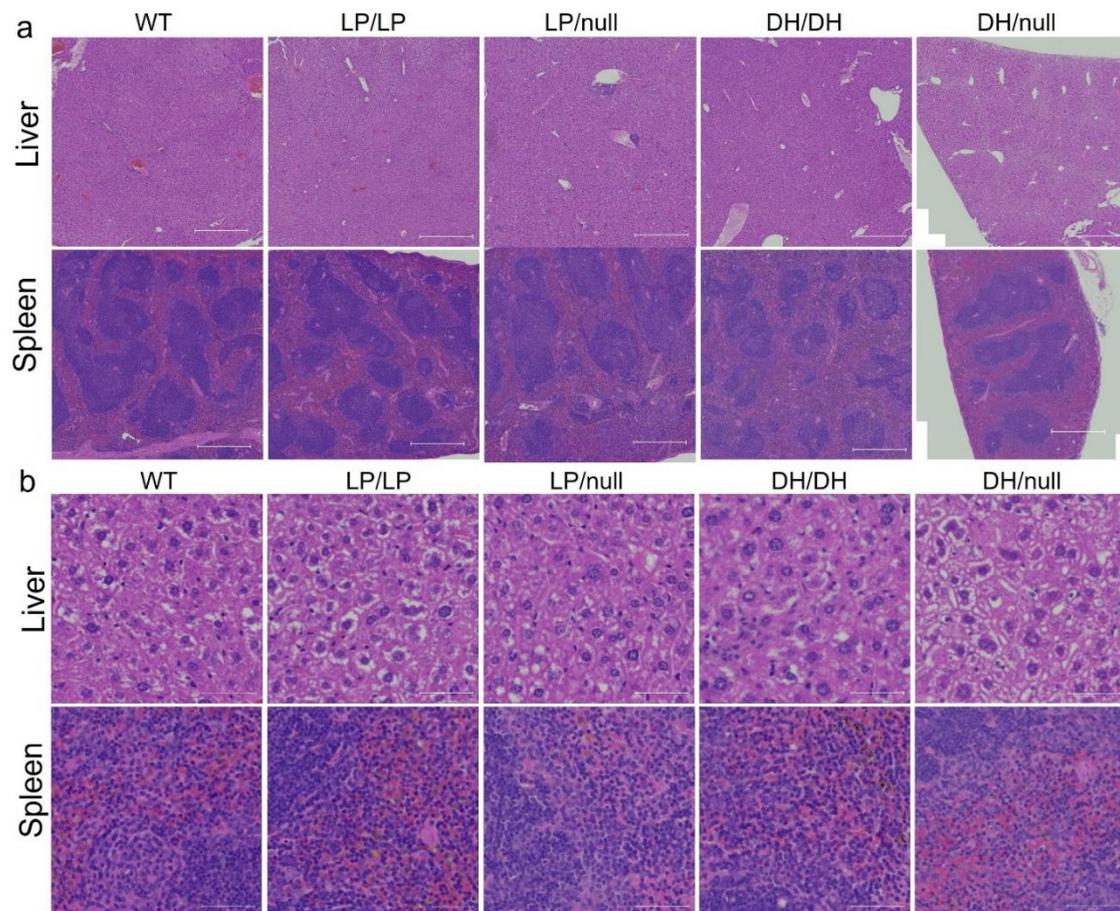
Figure 2. Histology evaluation of *Gba* mutant mice in liver and spleen. H&E staining was conducted in transverse section of liver or spleen tissue lysates from wildtype (WT), Gba[L444P/L444P] (LP/LP), Gba[L444P/null] (LP/null), Gba[D409H/D409H] (DH/DH), and Gba[D409H/null] (DH/null) animals. The staining was performed by Histoserv Inc using their general histology protocols. Images were collected by Zeiss Axioscan (a) H&E staining in the liver (top) and spleen (bottom) over a broad region. Scale bars, 500 μm. (b) H&E staining in the liver (top) and spleen (bottom) at higher magnification. Scale bars, 50 μm.

### 2.3. Evaluation of motor behavior in the L444P Gba mutant mice

While motor symptoms can be seen in patients with nGD and *GBA1*-associated PD s, assessment of the motor behavior of L444P and D409H homozygous mutant mice has not been previously reported. Since the L444P is a common *GBA1* mutation associated with PD, and the LP/LP mice showed both lipid accumulation and reduction of GCase protein levels (Figure 1), we tested the motor behavior of LP/LP mice compared with wildtype control mice. Motor balance was evaluated in 16-month-old mice using a the rotarod assay, but no significant differences in the latency to stay at acclimated rotarod speed was detected between LP/LP and WT mice (Figure 3a). A balance beam test was also performed using both a narrow beam (18 mm diameter) and a wide beam (24 mm), but no differences were noted in time to cross the beam between two groups with either beam width (Figure 3b and 3c). The complete motor behavior testing data are available in Zenodo at DOI: 10.5281/zenodo.10431016.
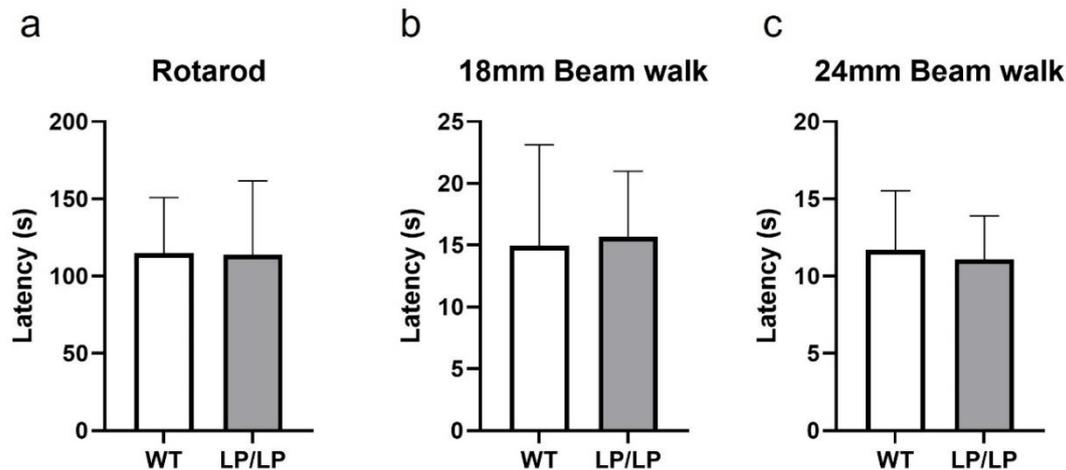
Figure 3. Evaluation of motor behavior in the Gba[L444P/L444P] mouse. (a) Rotarod testing. Latency until mice fail to walk on rotating rod was measured. (b) Balance beam testing using 18 mm diameter beam. Latency to cross the entire beam was measured. (c) Balance beam test using 24 mm diameter beam. Mice were tested at 16 months. WT is wildtype and LP/LP is *Gba[L444P/L444P]*. Ten mice of each genotype were evaluated. Error bars indicate the standard deviation. T-test was the statistical method used.

2.4. Evaluation of neuropathology in the Gba mutant mice

Since astrogliosis and microgliosis are common markers of CNS pathology detected in nGD and *GBA1*-associated PD, striatal tissue isolated from brain samples of aged mice with each genotype group were stained for Gfap and Iba1, respectively, and quantification of intensity was evaluated on the regions stained with each protein marker. While relatively higher levels of fibril staining of Gfap was detected in LP/null mice compared to the other genotypes, the differences did not reach statistical significance (Figure 4a and 4b). Also, there was no significant differences in Iba1 staining between five genotypes groups in striatal sections (Figure 4c and 4d). We also were not able to find any differences in cellular morphology in the Gfap and Iba1-stained cells regardless of genotype (Figure 4a and 4c). Midbrain sections harboring substantia nigra were also stained for tyrosine hydroxylase to evaluate dopaminergic neuronal loss, but no significant differences were detected between five genotypes (Figure 4e and 4f). All the immunohistochemistry quantification data are available in Zenodo at DOI: 10.5281/zenodo.10431016.
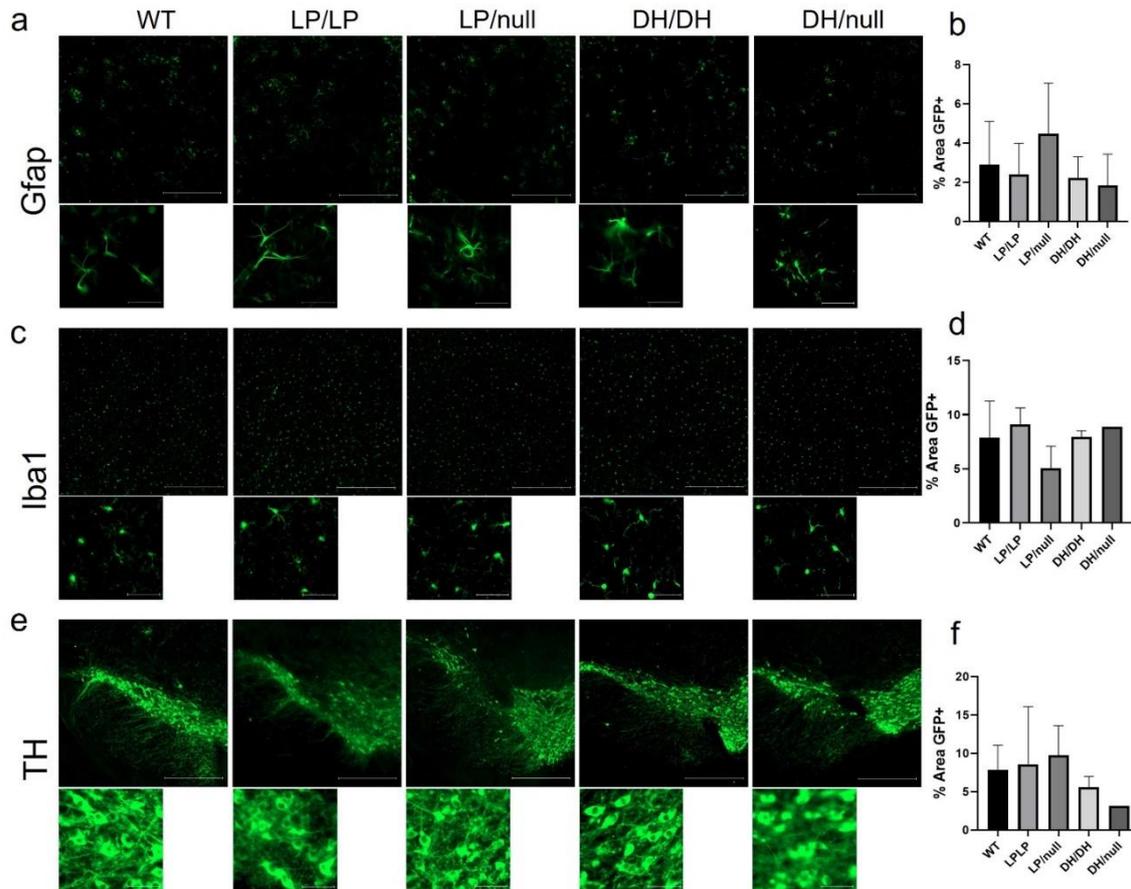
Figure 4. Evaluation of markers of neuropathology in brain from *Gba* mutant mice. Immunohistochemistry was conducted on brain sections from14-month-old wildtype (WT), *Gba*^L444P/L444P (LP/LP), *Gba*^L444P/null (LP/null), *Gba*^D409H/D409H (DH/DH), and *Gba*^D409H/null (DH/null) animals. (a) Gfap staining for astrocytes in striatal sections of brain from mice with each genotype (b) Quantificational analysis of Gfap staining in mice with each genotype. For WT N=4, LP/LP N=3, LP/null N=5, DH/DH N=4, and DH/null N= 2. (c) Iba1 staining for microglia in striatal sections of brain from mice with each genotype. (d) Quantificational analysis of Iba1 staining in mice with each genotype. For WT N=4, LP/LP N=3, LP/null, N= 4, DH/DH, N=2, DH/null, N=1. No statistics are available for the D409H/null animals because data is only available for one animal. (e) Tyrosine hydroxylase (TH) staining for DA neurons in the substantia nigra of mice with each genotype. (f) Quantificational analysis of TH staining in each genotype. For WT N=3, LP/LP N= 2, LP/null N=3, DH/DH N=2, and DH/null N=1. Scale bars in the upper images represent 500 µm and ln the lower images are 50 µm. Error bars indicate the standard deviation. One way ANOVA with Sidak's multiple comparison test was the statistical method used.

We evaluated the extent of α-synuclein levels in brain extracts of young adult (6-month-old) and older adult (14-month-old) mice. There was a trend towards greater accumulation in LP/LP and DH/null models compared to wildtype in the young adult mouse group, but this did not reach statistical significance (Figure 5a and 5b). There were no significant differences in α-synuclein levels between wildtype, DH/DH and LP/LP mice at 14 months (Figure 5c and 5d). All the immunoblot quantification data are available in Zenodo at DOI:10.5281/zenodo.10431048.
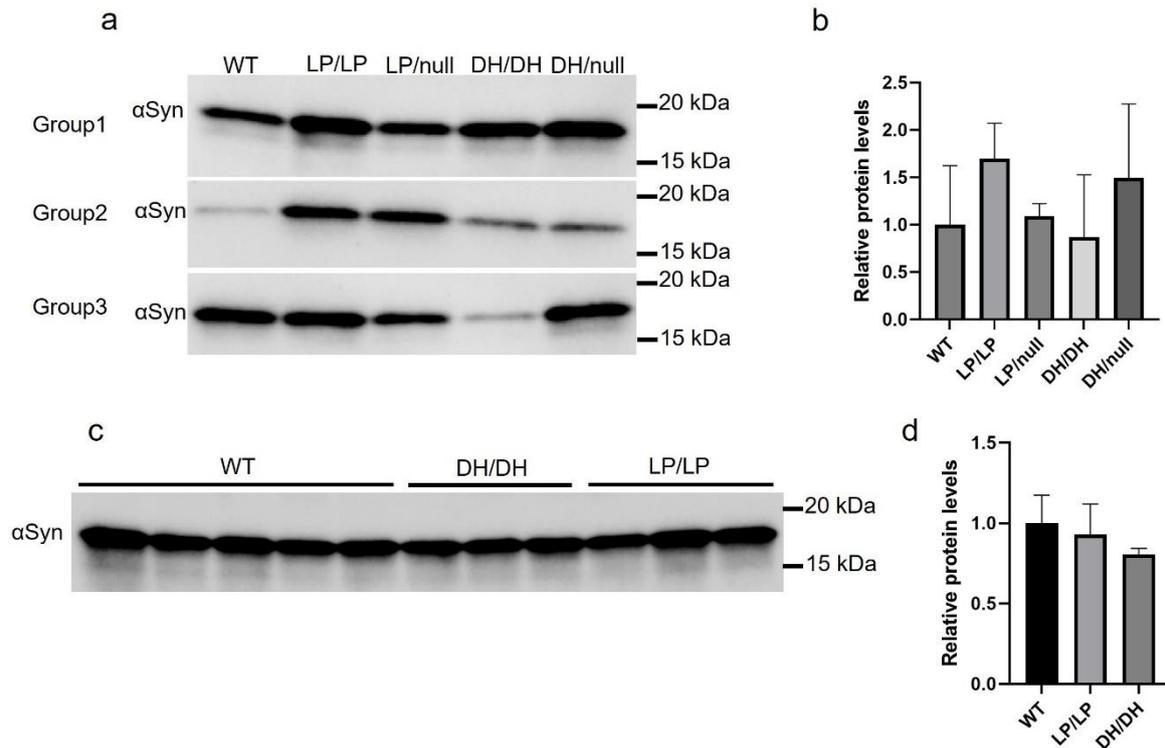
Figure 5. Evaluation of alpha-synuclein levels in brain samples from *Gba* mutant mice. Immunoblotting was conducted in brain lysates from wildtype (WT), *Gba*[L444P/L444P] (LP/LP), *Gba*[L444P/null] (LP/null), *Gba*[D409H/D409H] (DH/DH), and *Gba*[D409H/null] (DH/null) animals. All protein lysates were extracted from coronally cut mouse brain pieces harboring the cerebral cortex, basal ganglia, hippocampus, and midbrain. (a) Immunoblotting for total alpha-synuclein in RIPA-brain tissue lysates from 6-month-old animals. Size of band is approximately 15 kDa. The experiment was repeated in three different groups of animals including mice with each genotype. (b) Quantification of immunoblot data from 6-month-old animals. (c) Immunoblotting for total alpha-synuclein in RIPA-brain tissue lysates from 14-month-old animals. Experiment was repeated in 5 wildtype mice and 3 different DH/DH and LP/LP mice. (d) Quantification of immunoblot data from 14-month-old animals. Error bars indicate the standard deviation. One way ANOVA with Sidak's multiple comparison test was used for statistics.

3. Discussion

The four different *Gba* knock-in mice (LP/LP, LP/null, DH/DH and DH/null) evaluated as murine models of GD or *GBA1*-associated PD did not exhibit overt phenotypic manifestations encountered in these disorders despite having reduced glucocerebrosidase activity and some accumulation of glucosylsphingosine. Our findings confirm previous studies indicating that murine models of Gaucher disease show very mild to no phenotypic manifestations even though they exhibit reduced glucocerebrosidase activity. The *Gba* mutant mice did not differ in behavior, longevity, or fertility from age and sex-matched wildtype mice with the same genetic background. This observation suggests that introduction of an analogous *Gba* mutation is insufficient to induce the disease pathology observed in patients with GD.

The GCase activity in brain and liver from LP/LP and DH/DH mice was about 20-25% and 5-10% of wildtype respectively, which overall is consistent with previous reports, although it was surprising to see that the DH/DH mice showed lower activity than LP/LP mice, as this is not what is generally observed in patients with these genotypes. [14, 19, 23]. Increased levels of GlcSph were detected in both brain and livers of the LP/LP and DH/DH mice, although there was no change in GlcCer levels, consistent with previous reports [15, 22, 24]. The GCase activity was lower in liver than brain, corresponding to higher amounts GlcSph in liver than in brains in both L444P and D409H mice.

As reported in previous studies, the LP/LP mice had reduced GCase protein levels [25]. However, the previously reported reduced GCase levels described in DH/DH mouse brains [26] were not found in our study, and hence further replication studies are necessary to confirm the impact of the D409H mutation on GCase protein levels. Interestingly, D409H mutation carriers showed higher levels of GlcSph than L444P mutation carriers, while GCase activity was similar between the two. Mice with a combination of a null allele and missense mutation, as expected, had lower GCase activity levels than their homozygous counterparts, consistent with the finding that GlcSph levels in LP/null and DH/null were higher than that of LP/LP and DH/DH mice. However, despite the strong reduction of GCase activity and increased glycolipid accumulation, neither LP/null nor DH/null mice exhibited a noticeable pathological phenotype.

Remarkably, we did not observe histopathological changes in visceral tissues in any of the four *Gba* mutant lines, even with aging. Previous studies described rare Gaucher cells in liver and spleen of both LP/LP and DH/DH mice [18, 19] Furthermore the GlcSph levels in the LP/LP mice were lower than anticipated and it is not clear why our results differed from earlier reports. One possible explanation could be differences in strain background and cage conditions between studies. The DH/DH mice in our study may have a higher C57BL/6 (BL6) background ratio because the imported strain was rederived in the BL6 mice and backcrossed with the BL6 mice, while the DH/DH strain used in the previous study had a mixed background [19]. Additionally, none of these *Gba* models displayed neuroinflammation or other neuropathological findings. A previous study showed increased levels of astrocytes and alpha synuclein in striatum of LP/LP mice [18], which again was not replicated in our data. This could be due in part to our limited sample size which limited statistical quantification of the neuropathological images. It is also possible that the age at testing (14 months) is still not sufficient to enable detection of neuropathological phenotypes associated with neurodegeneration.

Another potential limitation is that the GCase activity assay used in this study was performed on whole tissue extract, and thus did not reflect what was specifically occurring in the lysosome. To better understand the impact of lysosomal GCase, newer GCase probes that function exclusively in the lysosome could potentially be used [27]. Another approach would be to breed our lines with lyso-tag mice engineered to carry a tag for lysosomal immunoprecipitation for tissue-specific isolation of intact lysosomes [28, 29].

The current study shows that mice carrying GD-causal mutations do not accurately recapitulate phenotypes detected in patients with GD. Since the *Gba* mutations resulted in significantly increased GlcSph levels yet did not result in pathological changes, even in aged mice, it appears that in the mouse, glycolipid accumulation alone is not sufficient to generate the phenotypes observed in human patients. One of possible explanation about this discrepancy is that in mice mechanisms such as the unfolded protein response (UPR) [30] has greater impact on disease pathogenesis than accumulation of lysosomal glycolipids alone. Thus, mutations L444P and D409H may not generate sufficient UPR to induce pathology in mice even though GCase activity is reduced, and glycolipid levels are increased. Another possibility is that lysosomal accumulation of glycolipid in mice is still below the threshold required for neuropathological progression. In these models, it appears that even low levels of GCase are enough to maintain normal homeostasis. Others have shown that in order to generate mouse models of GD with more prominent neuropathological features, it has been necessary to introduce a secondary burden such as under-expression of prosaposin [22], over-expression of pathological alpha-synuclein [26] or injection of pre-formed fibrils [24]. Several mouse models exhibiting a strong neurological phenotype have been developed using a conditional or induced *Gba* knock-out strategy [9, 31]. While such models are useful for the development of therapeutics such as gene therapy, they cannot be used to validate other strategies like small molecule chaperones. [32]. Thus, further studies and new strategies are necessary to develop more efficient animal model of GD with GD-causal missense mutations.

4. Materials and Methods

4.1. Mouse Lines

Gba^{L444P} mice were generated as previously described [18] (RRID:IMSR_JAX:024574). The details of the procedures used to generate the Gba^{L444P} strain are also described at DOI: dx.doi.org/10.17504/protocols.io.5jyl8p8qdg2w/v1. Subsequently, the neo cassette was removed by Cre driver. Sperm from D409H mice [22, 33] (RRID:MGI:7567849), was kindly provided by Dr. Ying Sun lab at Cincinnati Children's Hospital Medical Center, and live mice were rederived in the NHGRI Transgenic Mouse Core Facility by injecting sperm into C57BL/6 females (RRID:IMSR_JAX:000664). Homozygous mutants were generated by inbreeding of heterozygotes. Haploinsufficient mice (*Gba*+/-) [8], originated from the *Gba* knock line (RRID:IMSR_JAX:003321), were bred with L444P and D409H homozygotes to produce L444P/null (RRID:MGI:7567793) and D409H/null (RRID:MGI:7567850) animals. The total number of mice used in the study was 74 (WT:24, LP/LP:21, LP/null:10, DH/DH:12, DH/null:7). All housing and breeding of mice were performed under NHGRI Animal Care and Use Committee-approved protocols.

4.2. Motor Behavioral Evaluations

The rotarod test and beam-walk assay were used to evaluate the motor behavior of the different mice. Prior to rotarod testing, mice were acclimated to standing on a non-rotating rod (Rotamex 5, Columbus Instrument) for three 1-minute trials. Three hours later, mice were acclimated to walking on the rod over three 90 second trials at a speed of 4 rpm. After training, the instrument was set to begin at 4 rpm and gradually increase by 1 rpm every 8.33 second to a maximum speed of 40 rpm over 5 minutes. Mice were placed on the rod and the latency was recorded for three trials daily for two days. For the beam-walk assay, mice were trained to cross beams of 24mm and 18mm diameter. During training (over 2 days), each mouse crossed both beams three times. During the experimental day, mice crossed both beams twice per trial, for three trials. Latency to cross the beam was tracked with a stopwatch, and the number of foot slips during each crossing was counted. The details of the rotarod test and beam-walk assay procedures are described at DOI: dx.doi.org/10.17504/protocols.io.x54v9p5kqg3e/v1.

4.3. Tissue collection

At age 14 months, mice with each of the five genotypes (WT, LP/LP, DH/DH, LP/null, DH/null) were anesthetized with Avertin (1mL/25g body weight) and perfused transcardially according to standard NIH protocol (Whole Body Perfusion Fixation in Mice, v6, effective 8/27/2019) with 1x PBS (Quality Biological) containing 1 IU Heparin/mL, followed by 4% PFA for fixation. Brains were collected and post-fixed in 4% PFA at 4°C for 24 hours before being transferred to 30% sucrose for cryoprotection at 4°C for 24-48 hours, until the brain sank to the bottom of the vessel. The floating sections of brain were kept at 4° C for 8 weeks maximum for immunohistochemistry. Spleen and liver samples were collected using the same perfusion procedure for histological evaluations. After 24 hours of post-fixation, tissues were kept in 70% ethanol until paraffin embedding. For the GCase activity assays, lipid analysis and immunoblotting, brain (left and right hemispheres) and liver were collected after performing euthanasia in a CO_2 chamber, snap-frozen, and stored at -80° C. The details of the tissue collection procedures are described at DOI: dx.doi.org/10.17504/protocols.io.n2bvj3ejwlk5/v1.

4.4. Immunohistochemistry (IHC)

Brain tissue was sliced with a freezing sliding microtome (ThermoScientific HM450) at 30 μm and stored in 1x PBS with 0.1% sodium azide until needed. Selected sections were mounted on a slide (FischerBrand SuperFrost Plus) and were dried at room temperature for 30 minutes. A hydrophobic barrier was created around the tissue sections with a PAP pen (Newcomer Supply). Slides were rehydrated in 1x PBS for at least 10 minutes before blocking for 1 hour at room temperature in a solution of 15% Normal Goat Serum (Vector Laboratories) in 1x PBS with 2% Tween-20 (PBS-T). Diluted (10% Normal Goat Serum in PBS-T) primary antibodies (Gfap 1/1,000, Proteintech 16825-1-AP, RRID:AB_2109646; Iba1 1/400, Abcam ab178846, RRID:AB_2636859; TH 1/400, Sigma-Aldrich

AB152, RRID:AB_390204) were incubated overnight in a humidity chamber at 4°C and rinsed three times for 5 minutes with 1x PBS. Secondary antibody (1/400 Alexa-488, Abcam ab150077, RRID:AB_2630356) diluted in 10% Normal Goat Serum in PBS-T was added to the slides and incubated at room temperature for 2 hours. Slides were rinsed three times in 1x PBS for 5 minutes then topped with a coverslip (FischerBrand) with DAPI antifade medium (Vector Laboratories) and left at room temperature until dry (usually overnight). The details of IHC procedures are described at DOI: dx.doi.org/10.17504/protocols.io.6qpvr36yovmk/v1.

4.5. IHC Data Processing

Widefield fluorescent images were collected for GFP and DAPI fluorescent channels using a Zeiss AxioScan.Z1 slide scanning microscope system (Carl Zeiss Inc., Thornwood, NY, USA) with a Plan-Apochromat 20x/0.8 objective lens. All images were acquired using a Hamamatsu Orca flash 4.0 camera with an average tile count of 165 tiles per brain section. The Zeiss ZEN blue v.2.3 software package (https://www.zeiss.com/microscopy/en/products/software/zeiss-zen-lite.html#contact, RRID:SCR_013672) was used for collection and stitching of the 2-color (DAPI & GFP) tiled images. Widefield fluorescent images were then post-processed using MediaCybernetics' Image-Pro v.11 software package (https://mediacy.com/image-pro, RRID:SCR_016497). Every stitched image was processed using a protocol modified for each antibody. Initially, the image was masked to solely include the tissue in areas of interest. Then, Smart Segmentation was used to separate GFP-expressing puncta or fibrils from DAPI-stained nuclei in tissue evaluated with Gfap and anti-TH antibodies. Threshold segmentation was used for Iba1 staining to separate actual signal from background autofluorescence. Finally, the Count/Size function was designed to extract the percent of the tissue sample that stained positive for GFP. The details of IHC data processing procedures are described at DOI: dx.doi.org/10.17504/protocols.io.x54v9p5omg3e/v1.

4.6. GCase Activity Assays

GCase buffer (20 mL of 0.2M Na_2HPO_4 with 15 mL of 0.1M citrate adjusted to pH 5.4 with additional citrate as needed) was made and activated on the day of the assay (one Roche cOmplete mini tablet per 10mL buffer, 0.25% Triton X-100 and 0.2% sodium taurocholate). Protein lysates were prepared in a 96 well-plate, diluting samples with GCase buffer. The concentration of protein was determined via a BCA assay and control and experimental samples were maintained at similar concentrations (0.5-1mg/mL). 0.8 mM CBE was prepared by diluting 100mM CBE in GCase buffer. Control buffer without CBE was also prepared by mixing DMSO with GCase buffer (9.2:0.8 GCase buffer: DMSO). 10ul of protein lysate from the 96 well-plate was pipetted to each assay well in a 384 well-plate with four replications using an Eppendorf multichannel pipette. 5uL of 0.8mM CBE and 5uL of control buffer without CBE were added and incubated for 15 min at 37°C shaking at 600 rpm. 2.5 mM 4-Methylumbelliferyl-B-D-glucoside (4-MU) was prepared by diluting 1M 4-MU in GCase buffer. Following the 15 min incubation, the 384 well-plate was spun down and 15uL of 4-MU solution was added to each assay well to reach a total volume of 30uL per well and incubated for 1 hour at 37°C, shaking at 450 rpm. Following incubation, plates were spun down and 30uL of 1M glycine solution (pH 10.5) was added to each assay well. 4-MU fluorescence was read with a microplate reader (Flexstation 3, Molecular devices, Excitation: 365 nm; Emission: 449 nm; Cutoff: 435nm; 3 reads/well). GCase activity was calculated for each protein lysate according to the equation: (fluorescence of CBE-free sample minus fluorescence of sample with CBE) / protein concentration. The details of the GCase activity assay are described at DOI: dx.doi.org/10.17504/protocols.io.dm6gp3b7dvzp/v1.

4.7. GluCer and GluSph assays

The mouse brain and liver tissues (100 - 300 mg) were homogenized in 2% CHAPS solution (4 mL/g wet tissue) in 2 mL Omni homogenization tubes containing 8 mm ceramic beads. The homogenates were processed on the Bead Ruptor 24 (Omni International, Kennesaw, GA) for two 30

second cycles at 5.65 m/s with a 45 second pause time. The lipids glucosylsphingosine and glucosylceramide in the homogenate (50 µL) were extracted and analyzed using the liquid chromatography-tandem mass spectrometry methods as previously described [34]. The details of the lipid analysis are described at DOI: dx.doi.org/10.17504/protocols.io.261gedk8wv47/v2.

4.8. Immunoblotting

Protein lysates in RIPA buffer were treated with protease inhibitor and phosphatase inhibitor and diluted using the sample RIPA buffer to ensure equal concentrations for loading. 4X Leammli sample loading buffer (Biorad) with 10% β-mercaptoethanol was mixed with protein lysates and boiled at 99°C for 5 minutes. 20uL of each sample was loaded into TGX precast gels in Tris-Glycine-SDS buffer, along with 10uL of protein standard, and run for one hour at 120 V. Proteins were transferred to PVDF membranes using a Trans-Blot Turbo transfer system (Biorad). The membrane was dried for 30min, reactivated with 100% MeOH and rinsed with RO water. Ponceau S stain was added for 5 minutes and rinsed with RO water prior to imaging total proteins to normalize the data. After washing the membrane with buffer (1x TBS + 0.1% Tween 20) for 10 min, the membrane was incubated with blocking solution (2.5% milk mixed with 0.5x Intercept blocking buffer (LI-COR) in TBS) for 2 hrs while shaking. Primary antibody solution was prepared by diluting the antibody with the antibody dilution solution (2.5% milk mixed with 0.5x Intercept antibody diluent (LI-COR) in TBS). Blocking solution was replaced with antibody solution, and incubated overnight at 4°C. The membrane was washed three times for 10 min with a wash buffer. Secondary antibody at the same antibody dilution buffer concentration was incubated with the membrane for 1hr on the shaker at RT. After washing three times for 10 min, membranes were stained with ECL solution (SuperSiganal West Pico PLUS, Thermo Scientific) for 5 min and imaged with the Chemidoc MP (Biorad). Quantification of the images was performed using Image Lab software v.6.1 (https://www.bio-rad.com/en-us/sku/1709690-image-lab-software?ID=1709690, RRID:SCR_014210). The details of the Immunoblotting procedures are described at DOI: dx.doi.org/10.17504/protocols.io.3byl4qbnrvo5/v1.

4.9. Statistics

All experimental data were averaged for each genotype group and compared between groups using the statistical methods specified here. For the GCase activity assay, lipid assay, IHC and immunoblot results, an one way ANOVA test with Sidak's multiple comparison adjustment was used to obtain a statistical P-value for pairwise comparison of each group. For the motor behavioral evaluations, an unpaired T-test was used to compare the average of the two genotype groups. GraphPad PRISM v.9.5 (https://www.graphpad.com/features, RRID: SCR_002798) was used for all the statistical analyses.

help with training on the histological techniques, Dr Edward Ginns for generating the L444P mice, and Dr. Ying Sun for providing the D409H mice. We acknowledge the assistance of the NHGRI Embryonic Stem Cell and Transgenic Mouse Core, the NHGRI Cytogenetics and Microscopy Core and the NHGRI Animal Facility for animal care.

Conflicts of Interest: The authors declare that the research was conducted in the absence of any commercial or financial relationships that could be construed as potential conflict of interest.

References

1. Neudorfer, O.; Giladi, N.; Elstein, D.; Abrahamov, A.; Turezkite, T.; Aghai, E.; Reches, A.; Bembi, B.; Zimran, A., Occurrence of Parkinson's syndrome in type I Gaucher disease. *QJM* **1996,** *89,* 691-4.
2. Tayebi, N.; Walker, J.; Stubblefield, B.; Orvisky, E.; LaMarca, M. E.; Wong, K.; Rosenbaum, H.; Schiffmann, R.; Bembi, B.; Sidransky, E., Gaucher disease with parkinsonian manifestations: does glucocerebrosidase deficiency contribute to a vulnerability to parkinsonism? *Mol Genet Metab* **2003,** *79,* 104-9.
3. Grabowski, G. A.; Zimran, A.; Ida, H., Gaucher disease types 1 and 3: Phenotypic characterization of large populations from the ICGG Gaucher Registry. *Am J Hematol* **2015,** *90 Suppl 1,* S12-8.
4. Stirnemann, J.; Belmatoug, N.; Camou, F.; Serratrice, C.; Froissart, R.; Caillaud, C.; Levade, T.; Astudillo, L.; Serratrice, J.; Brassier, A.; Rose, C.; Billette de Villemeur, T.; Berger, M. G., A Review of Gaucher Disease Pathophysiology, Clinical Presentation and Treatments. *Int J Mol Sci* **2017,** *18.*
5. Farfel-Becker, T.; Vitner, E. B.; Futerman, A. H., Animal models for Gaucher disease research. *Dis Model Mech* **2011,** *4,* 746-52.
6. Cho, S. M.; Vardi, A.; Platt, N.; Futerman, A. H., Absence of infiltrating peripheral myeloid cells in the brains of mouse models of lysosomal storage disorders. *J Neurochem* **2019,** *148,* 625-638.
7. Cabasso, O.; Kuppuramalingam, A.; Lelieveld, L.; Van der Lienden, M.; Boot, R.; Aerts, J. M.; Horowitz, M., Animal Models for the Study of Gaucher Disease. *Int J Mol Sci* **2023,** *24.*
8. Tybulewicz, V. L.; Tremblay, M. L.; LaMarca, M. E.; Willemsen, R.; Stubblefield, B. K.; Winfield, S.; Zablocka, B.; Sidransky, E.; Martin, B. M.; Huang, S. P.; et al., Animal model of Gaucher's disease from targeted disruption of the mouse glucocerebrosidase gene. *Nature* **1992,** *357,* 407-10.
9. Enquist, I. B.; Lo Bianco, C.; Ooka, A.; Nilsson, E.; Mansson, J. E.; Ehinger, M.; Richter, J.; Brady, R. O.; Kirik, D.; Karlsson, S., Murine models of acute neuronopathic Gaucher disease. *Proc Natl Acad Sci U S A* **2007,** *104,* 17483-8.
10. Pewzner-Jung, Y.; Joseph, T.; Blumenreich, S.; Vardi, A.; Ferreira, N. S.; Cho, S. M.; Eilam, R.; Tsoory, M.; Biton, I. E.; Brumfeld, V.; Haffner-Krausz, R.; Brenner, O.; Sharabi, N.; Addadi, Y.; Salame, T. M.; Rotkopf, R.; Wigoda, N.; Yayon, N.; Merrill, A. H., Jr.; Schiffmann, R.; Futerman, A. H., Brain pathology and cerebellar purkinje cell loss in a mouse model of chronic neuronopathic Gaucher disease. *Prog Neurobiol* **2021,** *197,* 101939.
11. Farfel-Becker, T.; Do, J.; Tayebi, N.; Sidransky, E., Can GBA1-Associated Parkinson Disease Be Modeled in the Mouse? *Trends Neurosci* **2019,** *42,* 631-643.
12. Farfel-Becker, T.; Vitner, E. B.; Pressey, S. N.; Eilam, R.; Cooper, J. D.; Futerman, A. H., Spatial and temporal correlation between neuron loss and neuroinflammation in a mouse model of neuronopathic Gaucher disease. *Hum Mol Genet* **2011,** *20,* 1375-86.
13. Xu, Y. H.; Sun, Y.; Ran, H.; Quinn, B.; Witte, D.; Grabowski, G. A., Accumulation and distribution of alpha-synuclein and ubiquitin in the CNS of Gaucher disease mouse models. *Mol Genet Metab* **2011,** *102,* 436-47.
14. Liu, Y.; Suzuki, K.; Reed, J. D.; Grinberg, A.; Westphal, H.; Hoffmann, A.; Doring, T.; Sandhoff, K.; Proia, R. L., Mice with type 2 and 3 Gaucher disease point mutations generated by a single insertion mutagenesis procedure. *Proc Natl Acad Sci U S A* **1998,** *95,* 2503-8.
15. Mizukami, H.; Mi, Y.; Wada, R.; Kono, M.; Yamashita, T.; Liu, Y.; Werth, N.; Sandhoff, R.; Sandhoff, K.; Proia, R. L., Systemic inflammation in glucocerebrosidase-deficient mice with minimal glucosylceramide storage. *J Clin Invest* **2002,** *109,* 1215-21.
16. Fishbein, I.; Kuo, Y. M.; Giasson, B. I.; Nussbaum, R. L., Augmentation of phenotype in a transgenic Parkinson mouse heterozygous for a Gaucher mutation. *Brain* **2014,** *137,* 3235-47.
17. Taguchi, Y. V.; Liu, J.; Ruan, J.; Pacheco, J.; Zhang, X.; Abbasi, J.; Keutzer, J.; Mistry, P. K.; Chandra, S. S., Glucosylsphingosine Promotes alpha-Synuclein Pathology in Mutant GBA-Associated Parkinson's Disease. *J Neurosci* **2017,** *37,* 9617-9631.
18. Ginns, E. I.; Mak, S. K.; Ko, N.; Karlgren, J.; Akbarian, S.; Chou, V. P.; Guo, Y.; Lim, A.; Samuelsson, S.; LaMarca, M. L.; Vazquez-DeRose, J.; Manning-Bog, A. B., Neuroinflammation and alpha-synuclein accumulation in response to glucocerebrosidase deficiency are accompanied by synaptic dysfunction. *Mol Genet Metab* **2014,** *111,* 152-62.
19. Xu, Y. H.; Quinn, B.; Witte, D.; Grabowski, G. A., Viable mouse models of acid beta-glucosidase deficiency: the defect in Gaucher disease. *Am J Pathol* **2003,** *163,* 2093-101.

20. Abrahamov, A.; Elstein, D.; Gross-Tsur, V.; Farber, B.; Glaser, Y.; Hadas-Halpern, I.; Ronen, S.; Tafakjdi, M.; Horowitz, M.; Zimran, A., Gaucher's disease variant characterised by progressive calcification of heart valves and unique genotype. *Lancet* **1995,** *346*, 1000-3.

21. Kurolap, A.; Del Toro, M.; Spiegel, R.; Gutstein, A.; Shafir, G.; Cohen, I. J.; Barrabes, J. A.; Feldman, H. B., Gaucher disease type 3c: New patients with unique presentations and review of the literature. *Mol Genet Metab* **2019,** *127*, 138-146.

22. Sun, Y.; Quinn, B.; Witte, D. P.; Grabowski, G. A., Gaucher disease mouse models: point mutations at the acid beta-glucosidase locus combined with low-level prosaposin expression lead to disease variants. *J Lipid Res* **2005,** *46*, 2102-13.

23. Xu, Y. H.; Reboulet, R.; Quinn, B.; Huelsken, J.; Witte, D.; Grabowski, G. A., Dependence of reversibility and progression of mouse neuronopathic Gaucher disease on acid beta-glucosidase residual activity levels. *Mol Genet Metab* **2008,** *94*, 190-203.

24. Mahoney-Crane, C. L.; Viswanathan, M.; Russell, D.; Curtiss, R. A. C.; Freire, J.; Bobba, S. S.; Coyle, S. D.; Kandebo, M.; Yao, L.; Wan, B. L.; Hatcher, N. G.; Smith, S. M.; Marcus, J. N.; Volpicelli-Daley, L. A., Neuronopathic GBA1L444P Mutation Accelerates Glucosylsphingosine Levels and Formation of Hippocampal Alpha-Synuclein Inclusions. *J Neurosci* **2023,** *43*, 501-521.

25. Yun, S. P.; Kim, D.; Kim, S.; Kim, S.; Karuppagounder, S. S.; Kwon, S. H.; Lee, S.; Kam, T. I.; Lee, S.; Ham, S.; Park, J. H.; Dawson, V. L.; Dawson, T. M.; Lee, Y.; Ko, H. S., alpha-Synuclein accumulation and GBA deficiency due to L444P GBA mutation contributes to MPTP-induced parkinsonism. *Mol Neurodegener* **2018,** *13*, 1.

26. Kim, D.; Hwang, H.; Choi, S.; Kwon, S. H.; Lee, S.; Park, J. H.; Kim, S.; Ko, H. S., D409H GBA1 mutation accelerates the progression of pathology in A53T alpha-synuclein transgenic mouse model. *Acta Neuropathol Commun* **2018,** *6*, 32.

27. Cecioni, S.; Ashmus, R. A.; Gilormini, P. A.; Zhu, S.; Chen, X.; Shan, X.; Gros, C.; Deen, M. C.; Wang, Y.; Britton, R.; Vocadlo, D. J., Quantifying lysosomal glycosidase activity within cells using bis-acetal substrates. *Nat Chem Biol* **2022,** *18*, 332-341.

28. Laqtom, N. N.; Dong, W.; Medoh, U. N.; Cangelosi, A. L.; Dharamdasani, V.; Chan, S. H.; Kunchok, T.; Lewis, C. A.; Heinze, I.; Tang, R.; Grimm, C.; Dang Do, A. N.; Porter, F. D.; Ori, A.; Sabatini, D. M.; Abu-Remaileh, M., CLN3 is required for the clearance of glycerophosphodiesters from lysosomes. *Nature* **2022,** *609*, 1005-1011.

29. Abu-Remaileh, M.; Wyant, G. A.; Kim, C.; Laqtom, N. N.; Abbasi, M.; Chan, S. H.; Freinkman, E.; Sabatini, D. M., Lysosomal metabolomics reveals V-ATPase- and mTOR-dependent regulation of amino acid efflux from lysosomes. *Science* **2017,** *358*, 807-813.

30. Maor, G.; Cabasso, O.; Krivoruk, O.; Rodriguez, J.; Steller, H.; Segal, D.; Horowitz, M., The contribution of mutant GBA to the development of Parkinson disease in Drosophila. *Hum Mol Genet* **2016,** *25*, 2712-2727.

31. Enquist, I. B.; Nilsson, E.; Ooka, A.; Mansson, J. E.; Olsson, K.; Ehinger, M.; Brady, R. O.; Richter, J.; Karlsson, S., Effective cell and gene therapy in a murine model of Gaucher disease. *Proc Natl Acad Sci U S A* **2006,** *103*, 13819-24.

32. Chen, C.; Hertz, E.; Chen, Y.; Sidransky, E., Targeting protein clearance pathways in GBA1-associated Parkinson disease. *Expert Opin Ther Targets* **2022,** *26*, 1031-1035.

33. Sun, Y.; Grabowski, G. A., Impaired autophagosomes and lysosomes in neuronopathic Gaucher disease. *Autophagy* **2010,** *6*, 648-9.

34. Corado, C. R.; Pinkstaff, J.; Jiang, X.; Galban, E. M.; Fisher, S. J.; Scholler, O.; Russell, C.; Bagel, J. H.; PA, O. D.; Ory, D. S.; Vite, C. H.; Bradbury, A. M., Cerebrospinal fluid and serum glycosphingolipid biomarkers in canine globoid cell leukodystrophy (Krabbe Disease). *Mol Cell Neurosci* **2020,** *102*, 103451.